International Journal of Geo-Information

MDPI

Article

Examining Land Use/Land Cover Change and the Summertime Surface Urban Heat Island Effect in Fast-Growing Greater Hefei, China: Implications for Sustainable Land Development

Ying-ying Li [1,2], Yu Liu [2,3], Manjula Ranagalage [4,5], Hao Zhang [2,*] and Rui Zhou [6,*]

1 College of Forestry and Landscape Architecture, Anhui Agricultural University, Hefei 230036, China; lyyforward@ahau.edu.cn
2 Laboratory for Applied Earth Observation and Spatial Analysis (LAEOSA), Department of Environmental Science and Engineering, Jiangwan campus, Fudan University, 2005 Songhu Road, Yangpu District, Shanghai 200438, China; liuyu1982@henu.edu.cn
3 School of Civil Engineering and Architecture, Henan University, Kaifeng 475003, China
4 Department of Environmental Management, Faculty of Social Sciences and Humanities, Rajarata University of Sri Lanka, Mihintale 50300, Sri Lanka; manjularanagalage@ssh.rjt.ac.lk
5 Faculty of Life and Environmental Sciences, University of Tsukuba, 1-1-1, Tennodai, Tsukuba, Ibaraki 305-8572, Japan
6 School of Environmental and Geographical Sciences, Shanghai Normal University, 100 Guilin Road, Shanghai 200234, China
* Correspondence: zhokzhok@163.com or zhanghao_fdu@fudan.edu.cn (H.Z.); rzhou@shnu.edu.cn (R.Z.); Tel.: +86-21-31248919 (H.Z.); +86-21-64322447 (R.Z.)

Received: 24 August 2020; Accepted: 23 September 2020; Published: 29 September 2020

Abstract: In this study, a retrospective analysis of the relationship between the land use/land cover (LULC) change and associated surface urban heat island (SUHI) effect in fast-growing Greater Hefei between 1995 and 2016 was performed. Our results reveal the heterogeneous patterns of LULC change. The concentric buffer-based urban–rural gradient analysis reveals that most of the newly emerging developed land occurred within downtown Hefei. In contrast, in three suburban municipality/county jurisdictions, the overall area change in the non-developed land was much lower, but the net increase in developed land is remarkable. Meanwhile, the spatiotemporal patterns of SUHI are in good agreement with that of the developed land, as evidenced by the notable increase in SUHI intensity (SUHII) levels and SUHI spatial extent (SUHISE) in response to the rapid urban expansion, particularly along transportation corridors. In addition, partial least square regression (PLSR) models indicate that the buffer-based predictors/independent variables are significantly related to the responses (SUHII and SUHISE), explaining approximately 61.3% of the variance in the SUHII and 79.8% of the variance in the SUHISE, respectively. Furthermore, the relative strength of the independent variables in determining the relationship was quantitatively examined. The findings of this study provide clear evidence for decision making for sustainable land development and mitigation of the SUHI effect.

Keywords: land use/land cover change; surface urban heat island effect; partial least square regression; Greater Hefei; China

1. Introduction

During the past two centuries, urban areas have been the dominant human settlements globally, and approximately 68% of urban dwellers will live in the cities in 2050 [1]. However, among the consequences due to artificially altered hydrological circulation, climate regulation, soil conservation, and biodiversity

preservation [2–9], the urban heat island (UHI) effect, which is associated with human activities and climate change [10–12], has attracted increasing concern. Urban areas, which are subject to a local warming effect, or combined local and global warming effects, are the fundamental units for climate change adaptation and mitigation [13]. Thus, how cities cope with the UHI effect, particularly optimizing land use patterns towards sustaining regional ecosystems, will significantly affect UHI mitigation and adaption to climate change [14–20].

Since the late 1970s, China has been the largest urbanizing country in the world. The UHI effect has been one of the pronounced environmental problems, fueling growing concern among the public. Although the occurrence of the UHI effect is not necessarily proportional to urban size [21], numerous studies on the UHI effect have been focused on the leading megacities along the eastern coastal zones, which accommodate millions of migrants and have experienced dramatic urban growth. By comparison, case studies on the less-developed western and central cities are relatively scarce [22]. Recently, with the implementation of China's national strategies towards reducing the unbalanced development between the developed and less-developed regions [23,24], for the fast-growing big cities in the less-developed western and central regions, the linkage between their booming economic activities and the pronounced UHI effect has attracted more attention [25–27].

Two types of UHI effects have been investigated in previous research: the canopy UHI (CUHI) effect, which measures the rural–urban air temperature difference from in situ weather stations; and the surface UHI (SUHI) effect, which measures the rural–urban land surface temperature (LST) difference. Monitoring of the UHI effect has been undertaken with data retrieved from satellite remotely sensed thermal infrared (TIR) imagery [28,29]. The former approach has the advantage of a relatively long time-series of recorded data and high temporal resolution. Unfortunately, given the complicated urban morphology and changeable microclimatic factors, the sparse distribution of weather stations with low spatial coverage cannot sufficiently represent the CUHI effect of the whole city. Thus, this approach can be useful for retrospective analysis and prediction of the fine-scale CUHI effect but is biased at the city level. Alternatively, the satellite TIR imagery, which can capture the TIR signals of land surface with broad spatial coverage, has been widely used to examine the impacts of land use/land cover (LULC) change on the SUHI effect at city and regional levels [30–44]. The existing studies mostly emphasize the relationships between the LULC change and SUHI effect, using qualitative correlation analysis or quantitative methods (e.g., bivariate linear regression and multiple regression). Undoubtedly, the quantitative methods can provide more persuasive and convincing results. However, some questions arise from the application of the quantitative methods and the practical demands of decision making. Firstly, because most of the popular quantitative methods are based on the ordinary least-square (OLS) model, it remains a challenge to reveal the quantitative relationships between LULC change and the SUHI effect, considering these simple linear regression models may suffer from multicollinearity between the variables. Under such circumstance, stepwise regression cannot be a cure-all because removing the necessary independent variables may cause the loss of statistical power. Secondly, for a given regression model that contains multiple variables measured with different units, the issue of quantifying the relative importance of each independent variable and its influence on the SUHI effect has yet not been satisfactorily addressed. Thus, these debates must be clarified before the quantitative LULC change versus SUHI effect relationship can be adopted by decision makers engaged in sustainable urban land development and climatic adaption.

In this study, Greater Hefei, one of the star cities in central China and known as one of China's ten representative cities suffering from a pronounced summertime UHI effect [45], is suitable to be used to quantitatively examine the relationship between LULC change and summertime SUHI effect. The objective of the study is to achieve a better understanding of the relationship between LULC change and SUHI effect, and further provide valuable experience for urban planners and decision makers who are engaged in mitigating the SUHI effect and climate adaption for sustainable land development.

2. Study Region

Greater Hefei, the capital city of Anhui province, is situated in central China between latitudes 30°56′N–32°32′N and longitudes 116°40′E–117°58′E (Figure 1). This region has a northern subtropical humid monsoon climate, featuring mild temperatures in spring and autumn; a hot summer; and a cold winter. Its long-term recorded extreme temperatures are a maximum of 37.8~39.1 °C during the summer (from late June to early September) and a minimum of −9.9~−13.5 °C during the winter (from December to the following February), with an average annual temperature of 15.7 °C. Its precipitation averages 1000 mm/year, most of which occurs during May and August. Topographically, the city is located on the hilly terrain between the Yangtze River and the Huaihe River. The elevation ranges between 12 and 45 m above sea level.

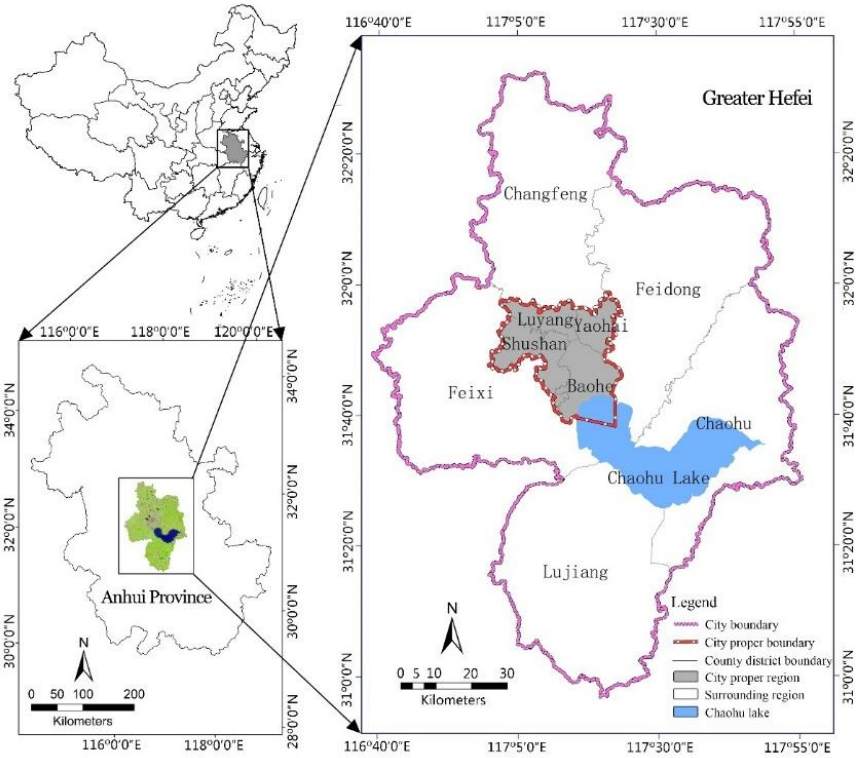

Figure 1. Location of the study region.

Hefei is an important city for its geographical advantage in central China, with a recorded history of 2200 years. It was one of the three cities that were first listed as China's National Garden Cities due to its natural landscape and splendid cultural heritage [46,47]. In 2011, the Greater Hefei region reshaped its boundary by merging with the former Chaohu city. Its administrative area almost doubled and the population increased by nearly 2 million. Its present administrative boundary consists of four districts (Luyang, Shushan, Baohe, and Yaohai), one municipality (Chaohu), and four counties (Feidong, Feixi, Changfeng, and Lujiang). It covers an area of approximately 11,430 km^2, with a total population of 7,965,000 [48]. Over the past decade, this region experienced an unprecedented rural–urban transition. With the implementation of industrial upgradation and trans-provincial relocation, intensive industrial parks and new settlements were developed at the periphery. However, the issue of coordinating land development plans, population growth, and mitigation of the UHI effect is absent from the official urban master planning documentation, given the extreme summertime heat events.

3. Materials and Methods

3.1. Data Sources

This study relies on the Landsat series images for retrieving LST data that indicate the summertime SUHI effect in Greater Hefei. Due to the limitation of weather conditions, the available Landsat series images with high quality and evenly annual intervals for this study are scarce. Therefore, multitemporal Landsat serial images (Level-1T, path 121/row 38) acquired during the summer period, including three Landsat Thematic Mapper (TM) images dated 1 August 1995, 11 July 2002, and 2 August 2007, and one Landsat Operational Land Imager (OLI)/Thermal Infrared Sensor (TIRS) image dated 25 July 2016, were used as the major dataset. All of the Landsat series images were free of cloud/haze contamination and released with terrain correction [49]. The auxiliary datasets include the commercial 30 m LULC maps (required on demand in 1995, 2002, 2007, and 2016) purchased from Beijing Digital Space Technology Co. Ltd, local socioeconomic data, and urban planning documents [46,47,50,51].

3.2. Methods

To clearly present the essential procedures for this study, an overall working flowchart, including data processing, LULC classification, LULC change measurement, retrieval of LST, and statistical analysis, is shown in Figure 2.

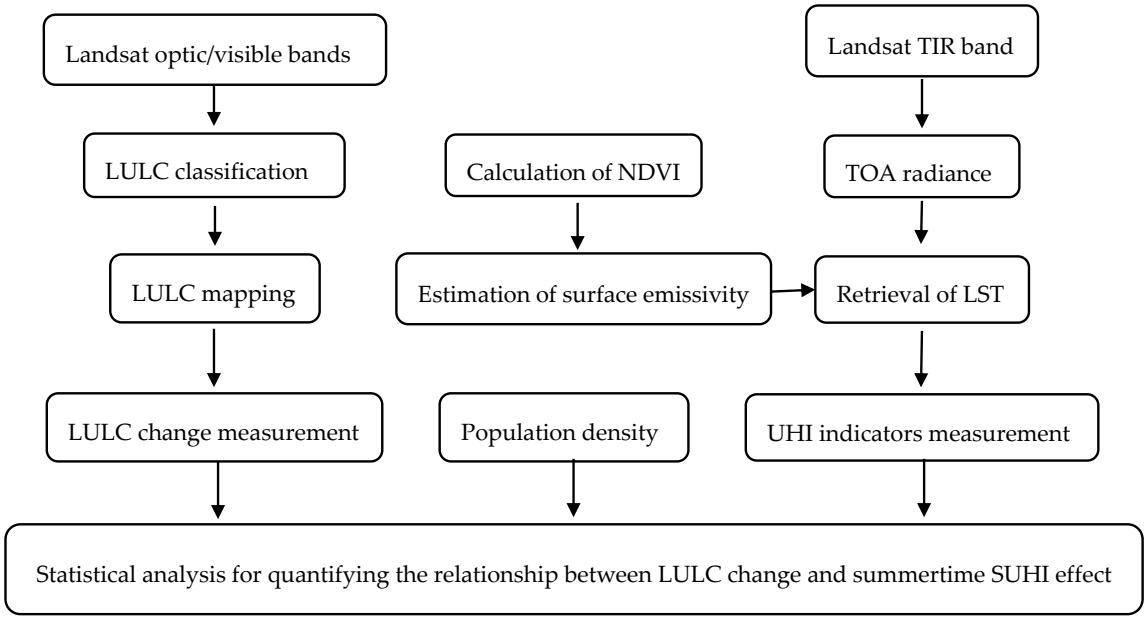

Figure 2. Overall working flowchart for this study.

3.2.1. Processing of Satellite Imagery

To obtain the overall LULC information for the study area, bands 5, 4, and 3 of Landsat TM were combined to generate false-color images. For Landsat OLI/TIRS image, bands 6, 5, and 4 were combined. Based on prior knowledge of Hefei urban planning materials and our field surveys, according to the guidance for national LULC classification [52], the LULC categories of this study region, namely developed land, forest, cropland, water body, and bare land, were adopted (Table 1). By overlapping commercial 30 m LULC maps (1995–2016), for each LULC type, at least 50 featured training sites were selected according to the random stratified sampling method. Thereafter, the supervised maximum likelihood classification method was used to perform LULC classification [53]. The 30 m commercial LULC maps acquired in 1995–2016 and field survey data in 2012–2016 were used for validating the classification results. To assess the accuracy of the classified results, for each image 250 samples

were randomly selected. The overall accuracy of LULC maps over the study period was determined to range from 73.7% to 92.6%, and the Kappa statistic ranged from 0.87 to 0.90, which met the value recommended by Jassen et al. [54].

Table 1. Land use/land cover (LULC) categories adopted in this study.

LULC Category	Description
Developed land	Urban and rural settlements, mainly including residences, commercial centers, economic development zone, industrial zones, college towns, railways, and highways
Forest	Mainly including natural and artificial woodlands, cropland shelterbelts, forest nurseries, and scrublands
Cropland	Paddy fields, fallow lands after harvest, drylands, and orchards
Water body	Lakes, rivers, ponds, reservoirs, fishponds, dikes, permanent and seasonal wetlands
Bare land	Bare rocks, quarries, mines, and vacant lands for urban development.

3.2.2. LULC Change Measurement

In this study, detection of LULC change was performed via overlapping time series of LULC maps and calculating the changed/unchanged pixels falling within each LULC category. To measure the LULC change under the pressure of rapid urbanization, particularly that attributable to human activities and socio-economic development along the rural–urban gradient, a series of concentric zonal buffers with different radii from the city center were drawn, based on our prior knowledge of the rural–urban transition and population growth of the study area. By analyzing the historical trends in population growth and urban encroachment in Greater Hefei, zonal buffers were drawn at 0–1.5, 1.5–3.0, 3.0–6.0, 6.0–12, 12.0–21.0, 21.0–33.0, 33.0–48.0, 48.0–66.0, and >66.0 km (66–100 km) from the city center (Table 2).

Table 2. Description of concentric buffers drawn along the urban–rural gradient.

Buffer Distance (km)	Description
0–1.5	The city core of downtown Hefei.
1.5–3.0	The urban area between the inner and the first ring roads.
3.0–6.0	The urban area between the first and second ring roads.
6.0–12.0	The urban area with intensive settlements, industrial parks, old airports, reservoirs, and national forest parks.
12.0–21.0	The rapidly urbanizing areas with intensive settlements, industrial parks, college towns, and new urban areas.
21.0–33.0	The rural areas with sparsely distributed towns and villages along with the traffic. This zonal buffer is characterized by cropland, Chao lake, reservoir, national forest park, a new airport, and river network.
33.0–48.0	The low-density developed rural areas with sparsely distributed towns and villages. This zonal buffer is characterized by cropland, Chao lake, hilly and mountainous terrain, and river network.
48.0–66.0	The low-density developed rural areas with sparsely distributed towns and villages. Aside from the well-developed urban area of Chaohu City, this zonal buffer is characterized by cropland and river networks.
>66.0	The low-density developed rural areas with sparsely distributed towns and villages. Aside from the well-developed urban area of Lujiang county in the south and Changfeng county in the east, this zonal buffer is characterized by hilly and mountainous terrain, dikes, and river network.

3.2.3. Retrieval of LST

In this study, the image-based method, which assumes uniform atmospheric condition and does not require thermal correction of the TIR band [55,56], was employed for retrieval of LST, given all the satellite images were free of cloud contamination. The detailed procedures for retrieval of LST included the following steps. Firstly, for Landsat TM images, prior to the retrieval of LST,

a quadratic model was used to convert the digital number (*DN*) of Landsat TM band 6 into brightness temperatures [57]:

$$T_B = 209.831 + 0.834DN - 0.00133DN^2, \quad (1)$$

For Landsat OLI TIR bands, because band 11 is subject to high uncertainty due to telescope stray light disturbance [58,59], band 10 was used to generated radiant temperatures as follows:

$$L_\lambda = gain \times DN + offset, \quad (2)$$

where L_λ is the radiance of thermal band pixels in W/(m^2 ster μm), gain is the slope of the radiance/*DN* conversion function, and offset is the slope of the radiance/*DN* conversion.

Secondly, for Landsat TM and Landsat 8 bands, the spectral radiance was then converted to at-satellite brightness temperature under the assumption of uniform emissivity [60].

$$T_B = \frac{K_2}{\ln\left(1 + \frac{K_1}{L_\lambda}\right)}, \quad (3)$$

where T_B is the effective at-satellite temperature in Kelvin (K), and both K_1 and K_2 are pre-launch calibration constants.

Thirdly, since the values of T_B were referenced to a black body rather than real earth objects, correction of spectral emissivity must be performed to retrieve the LST of true ground. It is currently a challenge to measure the emissivity values of the LULC types with remarkable variations. To reflect the spatially heterogeneous land surface emissivity, the emissivity of surface materials (ε) was calculated as follows [61]:

$$NDVI = \left(\frac{\rho_{NIR} - \rho_{Red}}{\rho_{NIR} + \rho_{Red}}\right) \quad (4)$$

$$P_v = \left(\frac{NDVI - NDVI_{\min}}{NDVI_{\max} - NDVI_{\min}}\right)^2 \quad (5)$$

$$\varepsilon = mP_v + n \quad (6)$$

$$m = (\varepsilon_v - \varepsilon_s) - (1 - \varepsilon_s)F\varepsilon_v \quad (7)$$

$$n = \varepsilon_s + (1 - \varepsilon_s)F\varepsilon_v \quad (8)$$

where *NDVI* denotes the normalized difference vegetation index, and ρ_{NIR} and ρ_{Red} denote the reflectance of the near-infrared band and the red band, respectively. P_v denotes the vegetation proportion, $NDVI_{\min}$ denotes the minimum value of *NDVI*, and $NDVI_{\max}$ denotes the maximum value of *NDVI* [62]. ε_v denotes vegetation emissivity and ε_s denotes soil emissivity. The values of m and n were referenced to the results of Sobrino et al. [61].

Furthermore, the emissivity corrected LST was computed as follows [63]:

$$T_s = \frac{T_B}{1 + (\lambda \times T_B/\alpha)\ln\varepsilon}, \quad (9)$$

where T_s is the surface radiant temperature in Kelvin (K), T_B is the black body temperature in Kelvin (K), λ is the centroid wavelength of emitted radiance (λ = 11.5 μm for Landsat TM band 6 and 10.895 μm for Landsat OLI/TIRS band 10), $\alpha = h\,c\,/\,K$ (1.438×10^{-2} mK), h is the Planck constant (6.626×10^{-34} J s^{-1}), c is the velocity of light (2.998×10^8 m s^{-1}), K is the Boltzman constant (1.38×10^{-23} J K^{-1}), and ε is the surface emissivity.

3.2.4. Measuring Summertime UHI Effect Indicators

In rapidly urbanizing areas, measurement of the routine UHI intensity based on the air temperature difference between urban and rural areas is problematic, largely due to the dramatic rural–urban

transformation that sharply altered the background air temperature [64,65]. Similarly, SUHI intensity measured by the LST difference between the urban and rural areas is also problematic. Alternatively, inspired by the concept of a local climate zone [65], measurement of the LST difference between the cooling surface (vegetated land and water bodies) and the impervious surface can better indicate the SUHI intensity and spatial extent influenced by the summertime SUHI effect. Therefore, based on the retrieved LST, two important summertime SUHI effect indicators, namely the SUHI intensity (SUHII) and spatial extent influenced by the SUHI effect (SUHISE), were measured as follows:

$$SUHII = LST_{IS} - LST_{CS}, \tag{10}$$

where *SUHII* is indicated with °C, LST_{IS} is the mean *LST* of the impervious surface within a given zonal buffer, and LST_{CS} is the mean *LST* of the cooling surface within a given zonal buffer.

$$SUHISE = \frac{P \cdot A}{10^6}, \tag{11}$$

where *SUHISE* is indicated with km^2, *P* is the total number of pixels (30 m resolution) with $SUHII \geq 0$, and *A* is the pixel-specific area.

Subsequently, based on our overall understanding of the spatiotemporal pattern of SUHI indicators of the study region, the SUHII was divided into six levels according to the thresholds of percentiles pinpointed on the normal distribution curve, that is, level 1: extreme low (≤5%); level 2: slightly low (5~25%); level 3: low to slightly high (25~50%); level 4: mediate high (50~75%); level 5: very high (75~95%); and level 6: extreme high(≥95%). Similarly, the *SUHISE* was divided into six levels according to the thresholds of percentiles pinpointed on the distribution curve.

3.2.5. Statistical Analysis

Procedures for data analysis, including descriptive statistics, normality test, and Pearson's product-moment correlation, were employed before quantifying the assumed relationship between the SUHI effect indicators and independent variables. The multicollinearity between the variables was detected according to the result of correlation analysis (see Appendix A Table A1). Therefore, to address the problem of multicollinearity that may cause misleading results, a partial least squares regression (PLSR) model, which combines features from and generalizes principal component analysis (PCA) and multiple linear regression [66], was employed to quantify the assumed relationship between the SUHI effect indicators and independent variables. Furthermore, to avoid the over-fitting problem and determine a reasonable model with the appropriate number of components that has good predictive ability, the leave-one-out (LOO) method was used for cross-validation, according to the criteria for selecting the models with the highest average predicted R^2 and the lowest average prediction sum of squares (PRESS) [66]. The validated PLSR models are written as follows:

$$SUHII = \alpha_1 + \beta_1 \cdot X_1 + \beta_2 \cdot X_2 + \beta_3 \cdot X_3 + \beta_4 \cdot X_4 + \beta_5 \cdot X_5 + \beta_6 \cdot X_6 + \varepsilon_1, \tag{12}$$

where α_1 is the intercept; $\beta_1 \sim \beta_6$ are the partial coefficients; and $X_1 \sim X_6$ are the area proportions of Developed land, Forest, Waterbody, Cropland, and Bare land within a given buffer zone, respectively. X_6 is the mean population density (Pop_density, unit: 1000 persons per km^2) within a given zonal buffer; ε_1 is the error term.

$$SUHISE = \alpha_2 + \beta'_1 \cdot X_1 + \beta'_2 \cdot X_2 + \beta'_3 \cdot X_3 + \beta'_4 \cdot X_4 + \beta'_5 \cdot X_5 + \beta'_6 \cdot X_6 + \varepsilon_2, \tag{13}$$

where α_2 is the intercept, $\beta'_1 \sim \beta'_6$ are the partial coefficients; and the definitions of $X_1 \sim X_6$ are the same as for Equation (12). ε_2 is the error term.

The statistical processes employed in this study were performed with R 3.6 [67] and the pls library [68].

4. Results

4.1. Synoptic Analysis of LULC Change at the Regional Level

Figure 3 shows the LULC change in Greater Hefei. The cropland decreased by 14.26% from 9019.55 km^2 in 1995 to 7732.96 km^2 in 2016. Meanwhile, the other four LULC categories present unevenly increasing trends, evidenced by the remarkable growth in developed land, which grew by 126.57% from 564.45 to 1278.88 km^2 in 1995–2016, followed by forest, which grew by 66.62% from 719.41 to 1198.67 km^2. Bare land grew by 21.44% from 35.49 to 46.75 km^2, with considerable annual variation in its area. In contrast, water bodies show a relatively slow but stable changing rate (7.82%), increasing from 1082.01 to 1166.65 km^2 during the study period. At the regional level, the dramatic increases in developed land and forest, and slight increases in bare land and water bodies, accompanied by a sharp decrease in cropland, should be of particular concern.

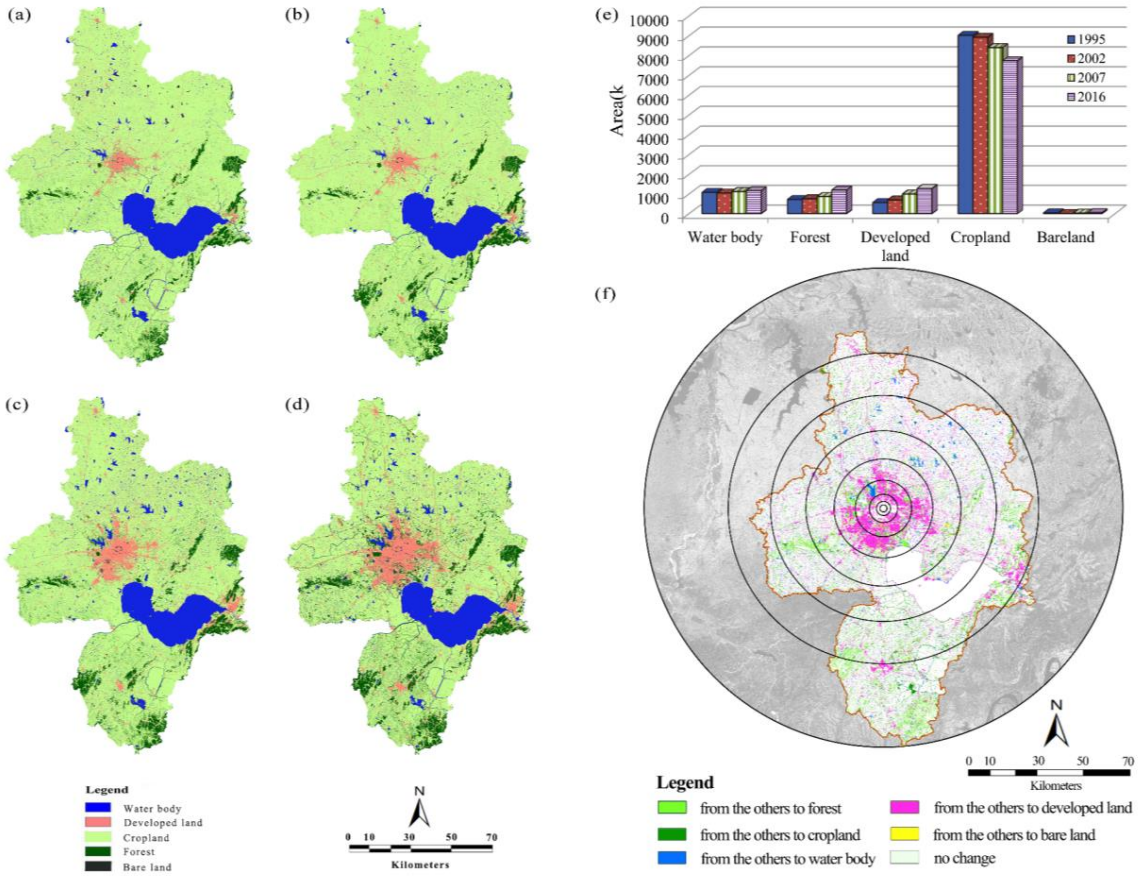

Figure 3. Land use/land cover (LULC) change in Greater Hefei during the study period. (**a**–**d**) show LULCs in 1995, 2002, 2007, and 2016, respectively; (**e**) shows the area of LULCs in 1995–2016; and (**f**) shows LULC conversion from other categories to the destined LULCs in 1995–2016 (Note: The concentric buffers were drawn according to the definition given in Table 2).

In addition, the heterogeneity of LULC change between the administrative zones of Greater Hefei is notable. As can be seen, most of the newly emerging developed land occurred within the extent of downtown Hefei. With the exception of the nearly unchanged old downtown within the first and the second buffers, the new extent of downtown Hefei, which falls between the third and fifth buffers, experienced a dramatic LULC change, as evidenced by 31.75% of newly emerging developed land, 29.59% of forest, and 20.28% of water bodies from other LULC categories. This result can be explained by the importance of administrative zones and their distance to downtown Hefei,

since the former city proper of Hefei dominated the outward expansion of developed land, and thus caused urban encroachment into the intensively developed land in neighboring Feidong and Feixi. In contrast, for the exurban counties and districts falling between the sixth and ninth buffers, the junior administrative importance, terrain constraints, and the far distance to downtown Hefei limit the intensive growth of developed land within their boundaries. Thus, the overall area changes in the non-developed land were considerably lower.

4.2. Change of Summertime SUHII and the Spatial Extent Influenced by SUHI Effect

Figures 4 and 5 show that the spatiotemporal patterns of summertime SUHI are in good agreement with that of the developed land (see Figure 2). The remarkable increase in SUHII levels and SUHISE can be attributed to the changing urban form and spatial linkage with neighboring county jurisdictions. As shown, in 1995–2000, the city proper dominates the spatial pattern of the intensively developed land at the regional level. The city proper exhibits much higher SUHII levels (4–6 levels within the 0–6 buffer zones) than the rest of the study region (1–6 levels). It is noteworthy that, since 2007, a mixture of in-filling and axial expansion occurred at the fringe of the city proper and eventually resulted in downtown Hefei, accompanied by increasing SUHII levels and SUHISE within the buffer zones (6–21 km). Furthermore, in marginal municipality/county jurisdictions (e.g., Chaohu, Lujiang, and Changfeng) and towns and villages within the transportation corridors, the significant increases in summertime SUHII levels and SUHISE can be observed. This indicates that the spatially close linkage between urban and rural developed land exerts a surface warming effect at regional and local levels. Besides, Figure 4 shows the overall trends in zonal SUHII and SUHISE along the urban–rural gradient. As shown, the urbanized and urbanizing areas within the 6–21 km buffer zones exhibit relatively higher summertime SUHII and SUHISE than the more distant buffer zones (>21 km). It appears the range of SUHII along the urban–rural gradient is smaller than that of the SUHISE. The spatial pattern of developed land can explain this result because most of the developed land is located within the 6–21 km buffer zones; in contrast, the area proportion of developed land in neighboring county jurisdictions is relatively small, and the dominant natural and semi-natural lands can help cool the land surface.

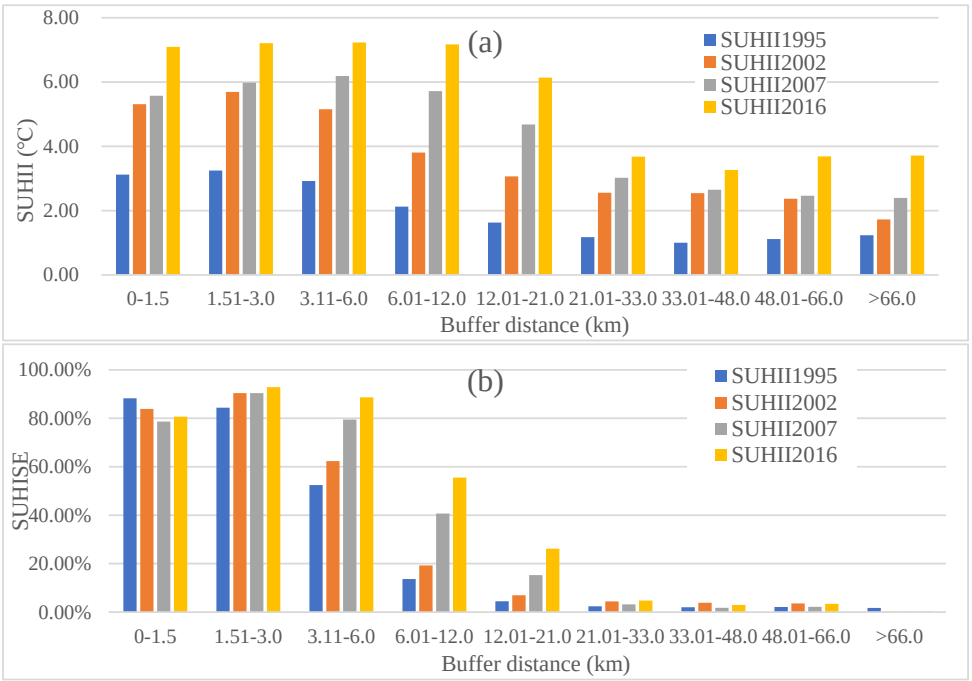

Figure 4. Zonal statistics of summertime SUHII (**a**) and SUHISE (**b**) in Greater Hefei during the study period.

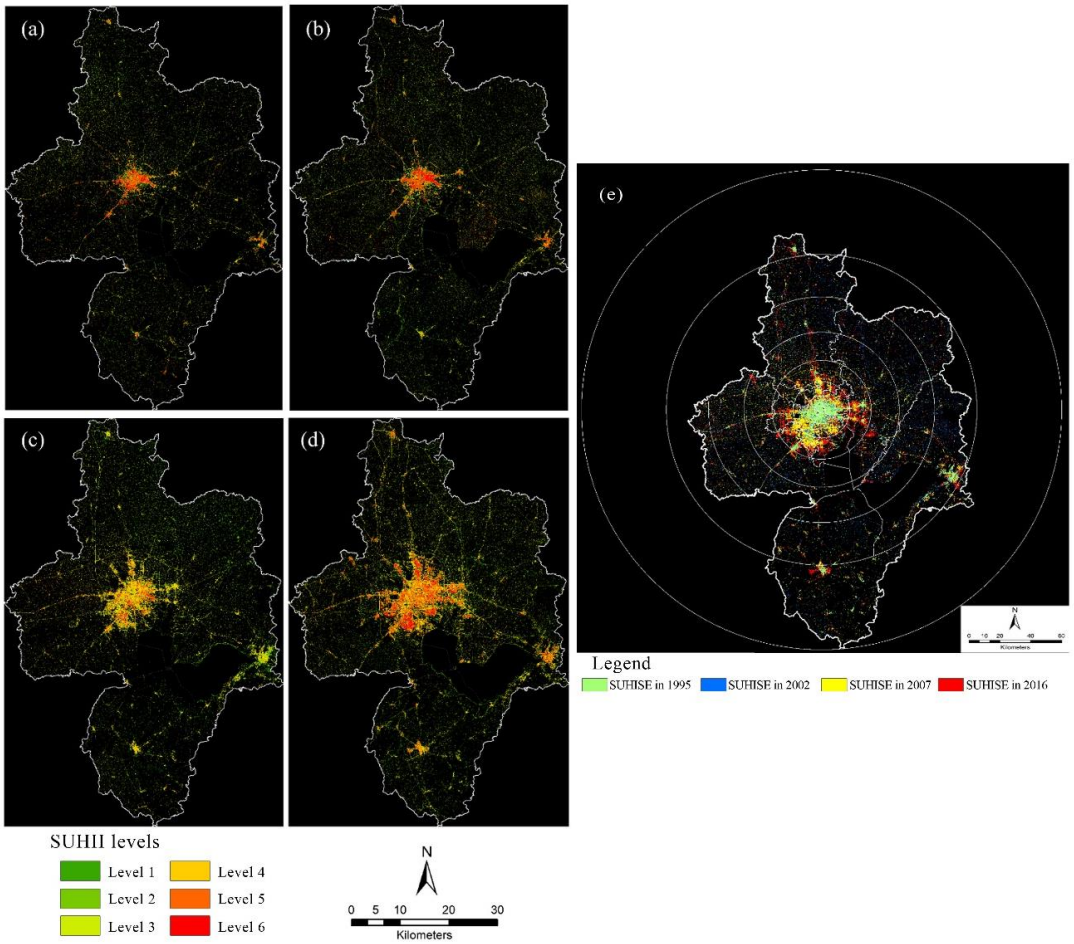

Figure 5. Spatiotemporal patterns of summertime surface urban heat island intensity (SUHII) levels in Greater Hefei dated (**a**) 1 August 1995; (**b**) 11 July 2002; (**c**) 2 August 2007; and (**d**) 25 July 2016; and (**e**) the sequential growth of SUHI spatial extent (SUHISE) in Greater Hefei during the study period. (Note: The dark pixels denote the non-developed land and the masked regions outside the study area).

4.3. Driving Factors Analysis of the Relationship between the LULC Change and SUHI Effect Indicators

Table 3 shows the overall relationships between the buffer-based predictors/independent variables and the responses (SUHII and SUHISE) in 1995–2016. The results of PLSR models indicate the independent variables are significantly related to the responses, explaining approximately 61.30% of the variance in the SUHII and 79.80% of the variance in the SUHISE within the study region. However, in addition to the annual and seasonal variations of the regional climate, the different units between the buffer-based LULC area proportions and population density make it difficult to directly compare the role of predictors in determining the variances of the responses. Alternatively, the standardized regression coefficients can better indicate the relative strength of the relationships between the buffer-based predictors/independent variables and the responses. Herein, the relative importance of the predictors was interpreted from two perspectives.

When focusing on the relationships between the buffer-based predictors/independent variables and the summertime SUHII, for the predictors with positive coefficients, the sequential order of the relative importance is Developed land > Bare land> Pop_density. As indicated, when controlling for the other independent variables, with each one standard deviation increase in Developed land, Bare land, and Pop_density, the resultant increases in the level of the SUHII standard deviations were 0.627, 0.221, and 0.098, respectively. Given the SUHII was measured with the LST difference between the LULC categories, the relative importance of Pop_density cannot be directly embodied via its standardized coefficient, although there is a highly significant correlation between developed land and Pop_density.

In contrast, for the predictors with negative coefficients, the sequential order of the relative importance is cropland > Water body > Forest. When controlling for the other independent variables, with each one standard deviation increase in Cropland, Water body, and Forest, the resultant decreases in the level of the SUHII standard deviations were 1.106, 0.16, and 0.104, respectively. Overall relationships between the buffer-based predictor variables and SUHISE were highly similar to the abovementioned buffer-based predictors versus SUHII relationships, except that the relative importance of Pop_density slightly surpasses that of Bare land. Such a change in the relative importance of Bare land can be explained by its thermal feature but small area proportion in the LULC categories.

Table 3. Coefficients of partial least squares regression (PLSR) models for summertime SUHII and SUHISE versus the independent variables.

	SUHII		**SUHISE**	
	Coefficients	**Standardized Coefficients**	**Coefficients**	**Standardized Coefficients**
Constant	6.724	0.000	53.813	0.000
Developed land	0.029	0.627	0.457	0.434
Forest	−0.201	−0.104	−0.286	−0.031
Water body	−0.065	−0.160	−3.735	−0.085
Cropland	−0.050	−1.016	−0.579	−0.518
Bare land	0.214	0.221	0.261	0.012
Pop_density	0.001	0.098	0.000	0.038
Summary statistics		$F_{4,31} = 19.499$, $p < 0.05$ $R^2 = 0.613$		$F_{4,31} = 47.290$, $p < 0.05$ $R^2 = 0.798$

5. Discussion

5.1. On the Relationship Between LULC Change and Summertime SUHI Effect

On local and regional scales, the occurrence of the SUHI effect in response to LULC change should be seen in the broad context of human activities rather than the LULC change itself. Both the biophysical features of the land surface and socioeconomic levels of the study areas play a critical role in causing LULC change and the associated SUHI effect. Most existing studies have focused on the relationship between the biophysical features of the land surface (e.g., NDVI, MNDWI, and NDBI) and associated SUHI effect [69,70]. Usually, due to the unavailability and uncertainty of socioeconomic variables, few studies have focused on the role of socioeconomic variables in determining the SUHI effect [44,71,72]. In some existing studies, ordinary least square (OLS)-based univariate and multiple linear regression models and non-linear regression models were employed to examine the simple and sophisticated relationships between LULC change and the SUHI effect, depending on the data availability and different research purposes. As previously noted, the univariate linear/non-linear regression models sometimes performed better, but the results of the multiple linear regression models were poorly interpreted when considering all of the potential variables that were assumed to be reasonable in the building the models [15,73]. However, this does not mean the failure of comprehensive models in this domain. PLSR is an explicit approach capable of removing multicollinearity among the variables by extracting from the predictors a set of orthogonal factors called latent variables which have the best predictive power [66]. In this study, we used PLSR models to examine the statistically significant relationships between the buffer-based independent variables and the dependent variables (SUHII and SUHISE), in addition to the relative importance of the independent variables in determining the complicated relationships. Nevertheless, the relative importance of Pop_density in contributing to the summertime SUHI effect indicators cannot be directly detected and thus may be underestimated, because of the simply measured LST difference between the impervious surface and cooling surface, and the lack of consideration of the interactions of the LULCs and Pop_density. Thus, we argue that a comprehensive model considering the joint influences of the biophysical features of LULCs and socioeconomic variables can help better understand the sophisticated relationships between

LULC change and the SUHI effect, given the existence of the noise of potential multicollinearity in the regression models.

5.2. Implications for Sustainable Land Development of a Better Urban Thermal Environment

Similar to the case of other big cities in central China, since the late 1970s, the socioeconomic development of Hefei has lagged behind that of the coastal megacities. This situation changed in 2002 when Greater Hefei implemented its development strategies for joining with the regional economic integration of the Yangtze river basin, through spatial development planning, urban agglomeration, industrial restructuring, and ecological conservation [74]. To date, most of these goals have been successfully achieved and laid the foundation for the expansion of Greater Hefei in the Yangtze River basin. In this study, as shown in Figure 2, the dramatic change in the expansion of downtown Hefei, which featured dense transportation corridors and an in-filling pattern of intensively developed land, largely reflected the LULC change in response to the land development pressure for the newly emerging high-tech parks, upgrading industrial clusters, supporting facilities, and residential communities.

Based on our results, it appears that the imbalance of the land development and population aggregation between the downtown Hefei and the marginal municipality/county jurisdictions should be responsible for the heterogeneity of LULC change and the summertime SUHI effect of the study region. Therefore, we argue that the relationship between the LULC change and associated SUHI effect should be stressed in the local authority's long-term plan actions and developmental strategies. For instance, the local authority can take advantage of the unprecedented opportunity provided by national strategies such as "Rise of central China", "Integration of the Yangtze river basin", and "Made in China 2025", which will favor internationally competitive industrial clusters, such as integrated circuits, new energy, intelligent connected vehicles, and quantum communication, in addition to the tertiary industry in Greater Hefei. However, it is notable that the local authority's recently issued plan (2018–2035) for these leading industrial clusters [75] prefers a site selection (491 km^2) within the 6–21 km buffer zones of downtown Hefei, given the convenience of livability and management. Nonetheless, no specific concerns on LULC change and the SUHI effect were embodied in the local authority's planning report, nor was there mention of a practical approach for suppressing the possible adverse thermal effect. It can be anticipated that such an intensive land developmental pattern will not only exacerbate land use competition for commercial development and ecological conservation, but will also not be helpful in shaping a balanced land development pattern between downtown Hefei and the marginal municipality/county jurisdictions. Consequently, the intensely developed land and over-dense population in downtown Hefei make it difficult to exploit sufficient space for spatially configured green spaces and water bodies for effective modification of the urban climate.

Thus, to alleviate the summertime SUHI effect in extreme heat events, future urban planning should reshape the urban form to suppress the over-intensive development in downtown Hefei and make room for cooling surfaces, by propagating the practices of ecological resilience and recovery to rebuild blue-green spaces across the urban–rural corridors. Based on our analysis of the present ecological land layout, we propose the planning of wetland parks and forest parks in the southeast and northwest parts of Greater Hefei, particularly to strengthen the protection zone of Chaohu Lake and optimize the low-impact development of the region. In addition, major ecological corridors, such as the Nanfei River ecological corridor and the Pai River ecological corridor, and the vast area of primary farmland area (for which urban development is permanently forbidden) should be incorporated into the ecological network to control the growth of construction land (see Figure 6).

5.3. Limitations of This Study and Remarks

Several minor limitations exist in this study. Theoretically, the time series of available satellite images may provide sufficient information for better understanding the process of LULC change and resultant levels of SUHII and SUHISE, which are highly important to decision making for sustainable land development, climate adaption, and ecosystem management. Unfortunately, due to cloud

contamination and the 16-day revisiting interval of Landsat satellites, the availability of satellite images with satisfactory quality is limited. Thus, the results of this study can only partially reveal the relationship between the LULC change and the associated daytime SUHI effect. Furthermore, the site-specific air temperature recorded at the weather stations should also be referenced for better representation of the spatiotemporal patterns of the summertime SUHI effect associated with LULC change. Usually, urban encroachment in suburban and rural areas causes bias in air temperatures at local weather stations, which is known as the "city-entering" phenomenon of stations [64]. However, when overlapping the LULC and summertime SUHI indicator maps with the weather stations map, and then reclassifying these weather stations to their correct suburban or rural area, the quantitative relationship between LULC change and SUHI effect discussed in this study will be more convincing.

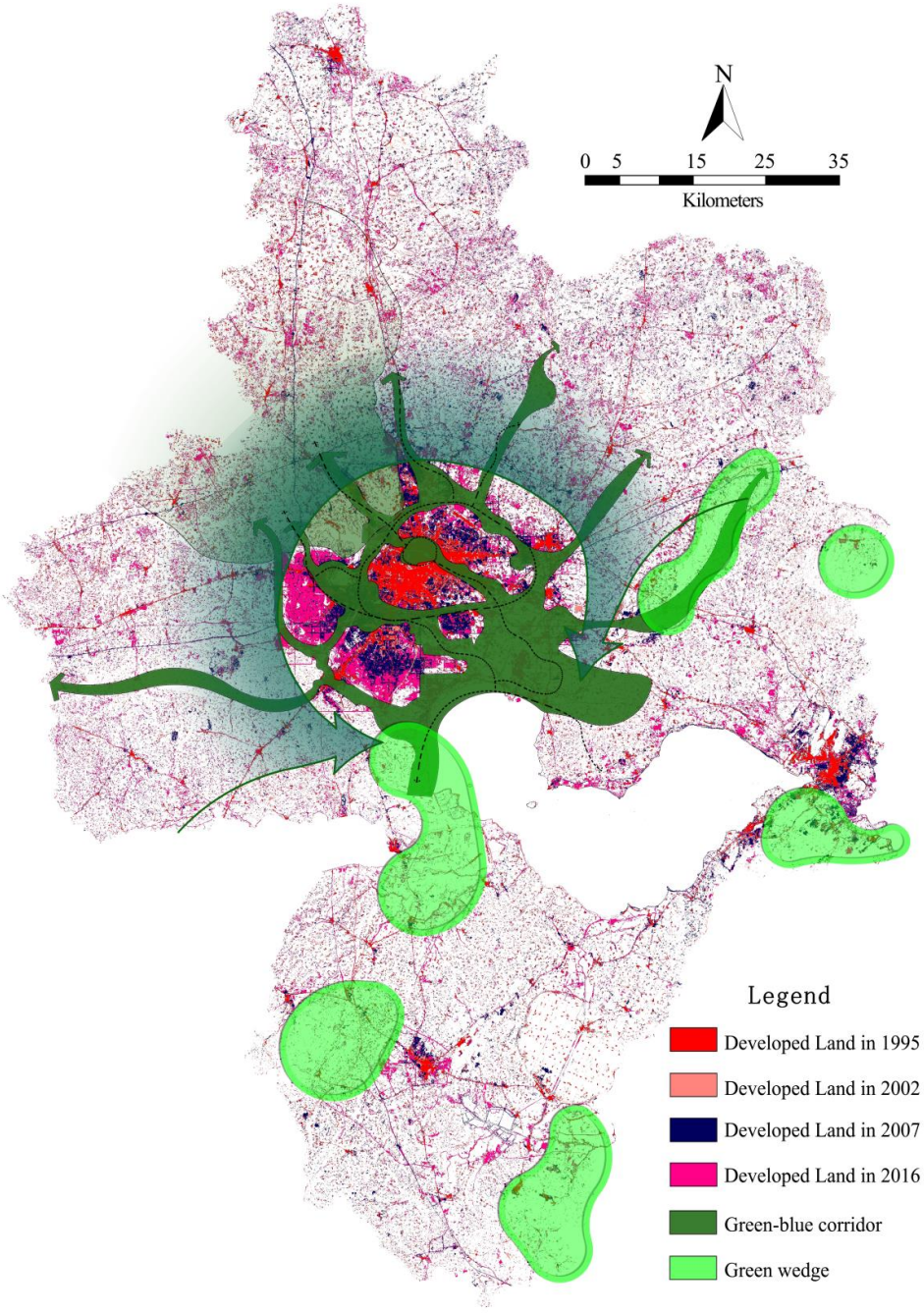

Figure 6. Proposed ecological network framework for mitigating the SUHI effect.

Another limitation is the relatively coarse resolution of the SUHI indicator products. The retrieved 30 m SUHI indicator products are suitable to depict the thermal effect of LULC change at medium and large scales with simple landscapes (e.g., forest, water bodies, cropland, and their mosaic), but they are insufficient to characterize the divergence in thermal effect of intensively developed land, especially in the relatively small-scale urban built environment with complicated LULC components and sophisticated urban morphology. Although no very high-resolution TIR band products are provided by the Landsat series satellite platforms, a few trial studies of thermal sharpening technology using a combination of Landsat TIR bands data and high-resolution satellite images have proven effective in monitoring the fine-scale SUHI effect in urban areas [76–78]. Moreover, the in situ measured air temperature and the CUHI effect cannot be directly compared with the SUHI effect. However, the combination of thermally sharpened SUHI effect indicators and in situ measured microclimatic factors can be used to generate the simulated CUHI indicators via computational fluid dynamics (CFD), which can be compared with the real CUHI indicators. Therefore, to enhance the applicability and feasibility of satellite remotely sensed TIR products in urban planning for UHI mitigation and climate adaption, more case studies using this thermal sharpening technology or similar methods should be encouraged.

6. Conclusions

In this study, the major findings can be summarized as follows.

(1) Overall, in Greater Hefei, the heterogeneous patterns of LULC change, particularly the noticeable differences in the growth patterns of the developed land between downtown Hefei and the marginal municipalities/counties, are observed. The centric buffer-based urban–rural gradient analysis reveals that most of the newly emerging developed land occurred within downtown Hefei, evidencing this city's transition from an ordinary provincial capital to a star megacity of central China during the past two decades. Consequently, the dramatic increase in developed land and slight increases in forest and water bodies caused a sharp decrease in cropland. In contrast, in three marginal municipality/county jurisdictions, the overall area change in non-developed land was much lower.

(2) The spatiotemporal patterns of summertime SUHI are in good agreement with that of the developed land. Rapid expansion of the developed land resulted in the remarkable increase in summertime SUHII levels and SUHISE. These were characterized by a mixture of in-filling and axial expansion along transportation corridors, or solely by axial expansion. The results of PLSR models indicate the zonal buffer-based predicators/independent variables are significantly related to the responses (SUHII and SUHISE), explaining approximately 61.3% of the variance in the SUHII and 79.8% of the variance in the SUHISE within the study region. In addition, the relative strength of the independent variables in determining the above-mentioned relationships was quantitatively examined. Therefore, optimization of the land development patterns is the key to mitigating the summertime SUHI effect and climatic adaption.

In summary, the findings of this study provide clear evidence for decision making toward sustainable land development and mitigating the pronounced summertime UHI effect.

Author Contributions: Hao Zhang and Rui Zhou conceived the central idea and designed the technical framework for this study. Ying-ying Li and Hao Zhang commanded data processing and analysis. Hao Zhang performed statistical analysis and wrote the manuscript. Manjula Ranagalage, Hao Zhang and Rui Zhou edited the draft manuscript. Yu Liu, Manjula Ranagalage, and Rui Zhou participated in discussing the findings of this study and helped enhance the research design, analysis, and manuscript writing. Specially, the authors are indebted to Conghe Song, who reviewed this manuscript and made rigid comments on enhancing the quality of this manuscript. All authors have read and agreed to the published version of the manuscript.

Funding: This study is jointly supported by the NSFC (Grants No. 41301650, 41401183 and 41730642), the Natural Science Foundation of Colleges, and Universities in Anhui Province (Grant No. KJ2019A0199), the Original and Innovatory Research Program (2017–2019) of Fudan University, the Natural Science Foundation of Shanghai (Grant No. 18ZR1427700), and the Humanity and Social Science Youth Foundation of the Ministry of Education of China (Grant No. 16YJCZH161).

Acknowledgments: The authors thank the USGS (http://www.earthexplorer.usgs.gov) for providing the Landsat series images. The authors are indebted to the R Foundation for Statistical Computing and Beijing Piesat Information Technology Co., Ltd. for free usage of the PIE 5.0 Remote Sensing image processing system.

Conflicts of Interest: There is no conflict of interest among authors.

Appendix A

Table A1. Correlation matrix indicating the multicollinearity between the variables.

	Developed Land	Forest	Water Body	Cropland	Bare Land	Pop_Density	SUHII
Forest	−0.642 **						
Water body	−0.272 *	0.576 **					
Cropland	−0.580 **	0.692 **	0.965 **				
Bare land	0.650 **	0.478 **	0.484 **	0.430 **			
Pop_density	0.484 **	−0.609 **	−0.654 **	−0.769 **	−0.372 *		
SUHII	0.611 **	−0.579 **	−0.602 **	−0.710 **	−0.234 *	0.705 **	
SUHISE	0.578 **	−0.634 **	−0.659 **	−0.785 **	−0.362 **	0.980 **	0.788 **

Note: * and ** denote significant at levels 0.01 and 0.05, respectively.

References

1. United Nations. 2018 Revision of World Urbanization Prospects. Available online: https://www.un.org/development/desa/publications/2018-revision-of-world-urbanization-prospects.html (accessed on 20 November 2018).
2. Cai, Y.-B.; Li, H.-M.; Ye, X.-Y.; Zhang, H. Analyzing three-decadal patterns of land use/land cover change and regional ecosystem services at the landscape level: Case study of two coastal metropolitan regions, eastern China. *Sustainability* **2016**, *8*, 773. [CrossRef]
3. Kim, J.J.; Ryu, J.H. Modeling Hydrological and Environmental Consequences of Climate Change and Urbanization in the Boise River Watershed, Idaho. *J. Am. Water Resour. Assoc.* **2019**, *55*, 133–153. [CrossRef]
4. Dewan, A.M.; Yamaguchi, Y. Land use and land cover change in Greater Dhaka, Bangladesh: Using remote sensing to promote sustainable urbanization. *Appl. Geogr.* **2009**, *29*, 390–401. [CrossRef]
5. King, R.S.; Scoggins, M.; Porras, A. Stream biodiversity is disproportionately lost to urbanization when flow permanence declines: Evidence from southwestern North America. *Freshw. Sci.* **2016**, *35*, 340–352. [CrossRef]
6. Nguyen, H.H.; Recknagel, F.; Meyer, W. Effects of projected urbanization and climate change on flow and nutrient loads of a Mediterranean catchment in South Australia. *Ecohydrol. Hydrobiol.* **2019**, *19*, 279–288. [CrossRef]
7. Mati, B.M.; Mutie, S.; Gadain, H.; Home, P.; Mtalo, F. Impacts of land-use/cover changes on the hydrology of the transboundary Mara River, Kenya/Tanzania. *Lakes Reserv. Res. Manag.* **2008**, *13*, 169–177. [CrossRef]
8. Pickard, B.R.; Van Berkel, D.; Petrasova, A.; Meentemeyer, R.K. Forecasts of urbanization scenarios reveal trade-offs between landscape change and ecosystem services. *Landsc. Ecol.* **2017**, *32*, 617–634. [CrossRef]
9. Reyers, B.; O'Farrell, P.J.; Cowling, R.M.; Egoh, B.N.; Le Maitre, D.C.; Vlok, J.H.J. Ecosystem services, land-cover change, and stakeholders: Finding a sustainable foothold for a semiarid biodiversity hotspot. *Ecol. Soc.* **2009**, *14*, 38. [CrossRef]
10. McMichael, A.J.; Woodruff, R.E.; Hales, S. Climate change and human health: Present and future risks. *Lancet* **2006**, *367*, 858–869. [CrossRef]
11. Jenerette, G.D.; Harlan, S.L.; Buyantuev, A.; Stefanov, W.L.; Declet-Barreto, J.; Ruddell, B.L.; Myint, S.E.; Kaplan, S.; Li, X. Micro-scale urban surface temperatures are related to land-cover features and residential heat related health impacts in Phoenix, AZ USA. *Landsc. Ecol.* **2016**, *31*, 745–760. [CrossRef]
12. Luan, X.; Yu, Z.; Zhang, Y.; Wei, S.; Miao, X.; Huang, Z.Y.X.; Teng, S.N.; Xu, C. Remote Sensing and Social Sensing Data Reveal Scale-Dependent and System-Specific Strengths of Urban Heat Island Determinants. *Remote Sens.* **2020**, *12*, 391. [CrossRef]

13. Georgescu, M.; Morefield, P.E.; Bierwagen, B.G.; Weaver, C.P. Urban adaptation can roll back warming of emerging megapolitan regions. *Proc. Natl. Acad. Sci. USA* **2014**, *111*, 2909–2914. [CrossRef] [PubMed]
14. Liu, J.; Shao, Q.; Yan, X.; Fan, J.; Zhan, J.; Deng, X.; Kuang, W.; Huang, L. The climatic impacts of land use and land cover change compared among countries. *J. Geogr. Sci.* **2016**, *26*, 889–903. [CrossRef]
15. Peng, J.; Jia, J.; Liu, Y.; Li, H.; Wu, J. Seasonal contrast of the dominant factors for spatial distribution of land surface temperature in urban areas. *Remote Sens. Environ.* **2018**, *215*, 255–267. [CrossRef]
16. Polydoros, A.; Mavrakou, T.; Cartalis, C. Quantifying the trends in land surface temperature and surface urban heat island intensity in mediterranean cities in view of smart urbanization. *Urban Sci.* **2018**, *2*, 16. [CrossRef]
17. Zhang, H.; Li, T.-T.; Liu, Y.; Han, J.-J.; Guo, Y.-J. Understanding the contributions of land parcel features to intra-surface urban heat island intensity and magnitude: Study on downtown Shanghai, China. *Land Degrad. Dev.* **2020**. [CrossRef]
18. Gill, S.; Handley, J.; Ennos, A.; Pauleit, S. Adapting Cities for Climate Change: The Role of the Green Infrastructure. *Built Environ.* **2007**, *33*, 115–133. [CrossRef]
19. Daily, G. *Nature's Services: Societal Dependence on Natural Ecosystems*; Island Press: Washington, DC, USA, 1997.
20. Dissanayake, D.; Morimoto, T.; Murayama, Y.; Ranagalage, M. Impact of Landscape Structure on the Variation of Land Surface Temperature in Sub-Saharan Region: A Case Study of Addis Ababa Using Landsat Data (1986–2016). *Sustainability* **2019**, *11*, 2257. [CrossRef]
21. Oke, T.R. City size and the urban heat island. *Atmos. Environ.* **1973**, *7*, 769–779. [CrossRef]
22. Ren, C.Y.; Wu, D.T.; Dong, S.C. The influence of urbanization on the urban climate environment in Northwest China. *Geogr. Res. Aust.* **2006**, *25*, 233–241.
23. China National People's Congress. The 10th Five-Year Plan Outline of China's for National Economic and Social Development. Available online: http://www.gov.cn/gongbao/content/2001/content_60699.htm (accessed on 1 November 2017).
24. The State Council of China. The 11th Five-Year Planning for Great Western Development Strategy. Available online: http://xbkfs.ndrc.gov.cn/qyzc/200901/t20090118_256835.html (accessed on 1 November 2017).
25. Wang, J.P.; Liu, J.; Du, J.S.; Zhang, X.; Xue, C.F.; Gao, W.Y. Interdecadal Variation of the Temperature and the Impact of Urban Growth on the Temperature in Xi'an Region. *Clim. Environ. Res.* **2009**, *14*, 434–444.
26. Cai, Z.; Han, G.F. Assessing land surface temperature in the mountain city with different urban spatial form based on local climate zone scheme. *Mt. Res.* **2018**, *4*, 617–627.
27. Zhao, H.; Zhang, H.; Miao, C.; Ye, X.; Min, M. Linking heat source–sink landscape patterns with analysis of urban heat islands: Study on the fast-growing Zhengzhou city in central China. *Remote Sens.* **2018**, *10*, 1268. [CrossRef]
28. Voogt, J.A.; Oke, T.R. Thermal remote sensing of urban climates. *Remote Sens. Environ.* **2003**, *86*, 370–384. [CrossRef]
29. Weng, Q. Thermal infrared remote sensing for urban climate and environmental studies: Methods, applications, and trends. *ISPRS J. Photogramm. Remote Sens.* **2009**, *64*, 335–344. [CrossRef]
30. Adinna, E.N.; Christian, E.I.; Okolie, A.T. Assessment of urban heat island and possible adaptations in Enugu urban using landsat-ETM. *J. Geogr. Reg. Plann.* **2009**, *2*, 30–36.
31. Keeratikasikorn, C.; Bonafoni, S. Urban heat island analysis over the land use zoning plan of Bangkok by means of landsat 8 imagery. *Remote Sens.* **2018**, *10*, 440. [CrossRef]
32. Rosenzweig, C.; Solecki, W.D.; Parshall, L.; Lynn, B.; Cox, J.; Goldberg, R.; Hodges, S.; Gaffin, S.; Slosberg, R.B.; Savio, P.; et al. Mitigating New York City's heat island: Integrating stakeholder perspectives and scientific evaluation. *Bull. Am. Meteorol. Soc.* **2009**, *90*, 1297–1312. [CrossRef]
33. Simwanda, M.; Ranagalage, M.; Estoque, R.C.; Murayama, Y. Spatial analysis of surface urban heat islands in four rapidly growing African cities. *Remote Sens.* **2019**, *11*, 1645. [CrossRef]
34. Rousta, I.; Sarif, M.O.; Gupta, R.D.; Olafsson, H.; Ranagalage, M.; Murayama, Y.; Zhang, H.; Mushore, T.D. Spatiotemporal analysis of land use/land cover and its effects on surface urban heat island using landsat data: A case study of metropolitan city Tehran (1988–2018). *Sustainability* **2018**, *10*, 4433. [CrossRef]
35. Sodoudi, S.; Shahmohamadi, P.; Vollack, K.; Cubasch, U.; Che-Ani, A.I. Mitigating the urban heat island effect in megacity Tehran. *Adv. Meteorol.* **2014**, *2014*. [CrossRef]

36. Lu, L.; Weng, Q.; Xiao, D.; Guo, H.; Li, Q.; Hui, W. Spatiotemporal Variation of Surface Urban Heat Islands in Relation to Land Cover Composition and Configuration: A Multi-Scale Case Study of Xi'an, China. *Remote Sens.* **2020**, *12*, 2713. [CrossRef]
37. Huang, Q.; Huang, J.; Yang, X.; Fang, C.; Liang, Y. Quantifying the seasonal contribution of coupling urban land use types on Urban Heat Island using Land Contribution Index: A case study in Wuhan, China. *Sustain. Cities Soc.* **2019**, *44*, 666–675. [CrossRef]
38. Qiao, Z.; Liu, L.; Qin, Y.; Xu, X.; Wang, B.; Liu, Z. The Impact of Urban Renewal on Land Surface Temperature Changes: A Case Study in the Main City of Guangzhou, China. *Remote Sens.* **2020**, *12*, 794. [CrossRef]
39. Singh, P.; Kikon, N.; Verma, P. Impact of land use change and urbanization on urban heat island in Lucknow city, Central India. A remote sensing based estimate. *Sustain. Cities Soc.* **2017**, *32*, 100–114. [CrossRef]
40. Tariq, A.; Riaz, I.; Ahmad, Z.; Yang, B.; Amin, M.; Kausar, R.; Andleeb, S.; Farooqi, M.A.; Rafiq, M. Land surface temperature relation with normalized satellite indices for the estimation of spatio-temporal trends in temperature among various land use land cover classes of an arid Potohar region using Landsat data. *Environ. Earth Sci.* **2020**, *79*, 40. [CrossRef]
41. Yang, C.; He, X.; Yan, F.; Yu, L.; Bu, K.; Yang, J.; Chang, L.; Zhang, S. Mapping the Influence of Land Use/Land Cover Changes on the Urban Heat Island Effect—A Case Study of Changchun, China. *Sustainability* **2017**, *9*, 312. [CrossRef]
42. Zhang, Y.; Sun, L. Spatial-temporal impacts of urban land use land cover on land surface temperature: Case studies of two Canadian urban areas. *Int. J. Appl. Earth Obs.* **2019**, *75*, 171–181. [CrossRef]
43. Liu, Y.; Peng, J.; Wang, Y. Application of partial least squares regression in detecting the important landscape indicators determining urban land surface temperature variation. *Landsc. Ecol.* **2018**, *33*, 1133–1145. [CrossRef]
44. Zhang, H.; Qi, Z.F.; Ye, X.-Y.; Cai, Y.B.; Ma, W.C.; Chen, M.-N. Analysis of land use/land cover change, population shift, and their effects on spatiotemporal patterns of urban heat islands in metropolitan Shanghai, China. *Appl. Geogr.* **2013**, *44*, 121–133. [CrossRef]
45. China Meterological Administration (CMA). The Increasing Trends of Hot Cities in China. Available online: http://www.cma.gov.cn/2011xwzx/2011xqhbh/2011xdtxx/201208/t20120816_182112.html (accessed on 11 November 2017).
46. Hefei Municipal Government. *Urban Master Planning of Hefei (2011–2020)*; Hefei Municipal Government: Hefei, China, 2012.
47. Hefei Municipal Government. *Overall Plan for Land Utilization of Hefei (2006–2020)*; Hefei Municipal Government: Hefei, China, 2012.
48. Hefei Municipal Statistics Bureau. The 2017 Report of Demographic Census in Hefei. Available online: http://tjj.hefei.gov.cn/8726/8730/201802/t20180223_2481649.html (accessed on 5 September 2019).
49. USGS. Available online: https://www.usgs.gov/centers/eros/science/usgs-eros-archive-landsat-archives-landsat-8-oli-operational-land-imager-and?qt-science_center_objects=0#qt-science_center_objects (accessed on 1 August 2019).
50. Anhui Provincial Statistics Bureau. The Annual Statistical Yearbook of Anhui Province. Available online: http://tjj.ah.gov.cn/tjjweb/web/tjnj_view.jsp?strColId=13787135717978521&_index=1 (accessed on 3 September 2019).
51. Hefei Municipal Statistics Bureau. The Annual Statistical Yearbook of Hefei. Available online: http://tjj.hefei.gov.cn/8688/8689/18nj/ (accessed on 5 September 2018).
52. China National Committee of Agricultural Divisions. *Technical Regulation of Investigation on Land Use Status*; Surveying and Mapping Publishing House: Beijing, China, 1984.
53. Chen, D.; Stow, D. The effect of training strategies on supervised classification at different spatial resolutions. *Photogramm. Eng. Remote Sens.* **2002**, *68*, 1155–1162.
54. Jassen, L.I.F.; Frans, J.M.; Wel, V.D. Accuracy assessment of satellite derived land-cover data: A review. photogramm. *Eng. Remote Sens.* **1994**, *60*, 410–432.
55. Song, C.; Woodcock, C.E.; Seto, K.C.; Lenney, M.P.; Macomber, S.A. Classification and change detection using Landsat TM data: When and how to correct atmospheric effects? *Remote Sens. Environ.* **2001**, *75*, 230–244. [CrossRef]
56. Weng, Q. A remote sensing-GIS evaluation of urban expansion and its impact on surface temperature in the Zhujiang Delta, China. *Int. J. Remote Sens.* **2001**, *22*, 1999–2014.

57. Malaret, E.; Bartolucci, L.A.; Lozano, D.F.; Anuta, P.E.; McGillem, C.D. Landsat-4 and Landsat-5 Thematic Mapper data quality analysis. *Photogramm. Eng. Remote Sens.* **1985**, *51*, 1407–1416.
58. Barsi, J.A.; Schott, J.R.; Hook, S.J.; Raqueno, N.G.; Markham, B.L.; Radocinski, R.G. Landsat-8 Thermal Infrared Sensor (TIRS) vicarious radiometric calibration. *Remote Sens.* **2014**, *6*, 11607–11626. [CrossRef]
59. Montanaro, M.; Gerace, A.; Lunsford, A.; Reuter, D. Stray light artifacts in imagery from the Landsat 8 thermal infrared sensor. *Remote Sens.* **2014**, *6*, 10435–10456. [CrossRef]
60. Department of the Interior/U.S. Geological Survey (DOI/USGS). The Landsat 8 (L8) Data Users Handbook (Version 4.0). EROS Sioux Falls, South Dakota. 2019. Available online: https://prd-wret.s3-us-west-2.amazonaws.com/assets/palladium/production/atoms/files/LSDS_1574_L8_Data_Users_Handbook_v4.pdf (accessed on 12 May 2019).
61. Sobrino, J.A.; Jiménez-Muñoz, J.C.; Paolini, L. Land surface temperature retrieval from Landsat TM 5. *Remote Sens. Environ.* **2004**, *90*, 434–440. [CrossRef]
62. Carlson, T.N.; Ripley, D.A. On the relation between NDVI, fractional vegetation cover, and leaf area index. *Remote Sens. Environ.* **1997**, *62*, 241–252. [CrossRef]
63. Artis, D.A.; Carnahan, W.H. Survey of emissivity variability in thermography of urban areas. *Remote Sens. Environ.* **1982**, *12*, 313–329. [CrossRef]
64. Yang, Y.J.; Wu, B.W.; Shi, C.E.; Zhang, J.H.; Li, Y.B.; Tang, W.A.; Wen, H.Y.; Zhang, H.Q.; Shi, T. Impacts of urbanization and station-relocation on surface air temperature series in Anhui Province, China. *Pure Appl. Geophys.* **2013**, *170*, 1969–1983. [CrossRef]
65. Stewart, I.D.; Oke, T.R. Local Climate Zones for Urban Temperature Studies. *Bull. Am. Meteorol. Soc.* **2012**, *93*, 1879–1900. [CrossRef]
66. Abdi, H. Partial least squares regression and projection on latent structure regression (pls regression). *Wiley Interdiplinary Rev. Comput. Stats* **2010**, *2*, 97–106. [CrossRef]
67. R Core Team. R: A Language and Environment for Statistical Computing. R Foundation for Statistical Computing, Vienna, Austria. 2019. Available online: https://www.R-project.org/ (accessed on 1 May 2019).
68. Mevik, B.-H.; Wehrens, R. The pls package: Principal component and partial least squares regression in R. *J. Stat. Softw.* **2007**, *18*, 1–24. [CrossRef]
69. Weng, Q.; Lu, D.; Schubring, J. Estimation of land surface temperature–vegetation abundance relationship for urban heat island studies. *Remote Sens. Environ.* **2004**, *89*, 467–483. [CrossRef]
70. Xu, H. Analysis of impervious surface and its impact on urban heat environment using the normalized difference impervious surface index (NDISI). *Photogramm. Eng. Remote Sens.* **2010**, *76*, 557–565. [CrossRef]
71. Buyantuyev, A.; Wu, J. Urban heat islands and landscape heterogeneity: Linking spatiotemporal variations in surface temperatures to land-cover and socioeconomic patterns. *Landsc. Ecol.* **2010**, *25*, 17–33. [CrossRef]
72. Guo, Y.J.; Han, J.J.; Zhao, X.; Dai, X.Y.; Zhang, H. Understanding the Role of Optimized Land Use/Land Cover Components in Mitigating Summertime Intra-Surface Urban Heat Island Effect: A Study on Downtown Shanghai, China. *Energies* **2020**, *13*, 1678. [CrossRef]
73. Tang, J.; Di, L.; Xiao, J.; Lu, D.; Zhou, Y. Impacts of land use and socioeconomic patterns on urban heat Island. *Int. J. Remote Sens.* **2017**, *38*, 3445–3465. [CrossRef]
74. Cai, Z. The strategic planning for spatial development of Hefei City. *Urban Plann. Newsrep.* **2005**, 14–15.
75. Huang, Q.H.; Li, M.C.; Liu, Y.X.; Hu, W.; Liu, M.; Chen, Z.J.; Li, F.X. Using construction expansion regulation zones to manage urban growth in Hefei City, China. *J. Urban Plan. Dev.* **2012**, *139*, 62–69. [CrossRef]
76. Bonafoni, S.; Anniballe, R.; Gioli, B.; Toscano, P. Downscaling Landsat land surface temperature over the urban area of Florence. *Eur. J. Remote Sens.* **2016**, *49*, 553–569. [CrossRef]
77. Zhang, H.; Jing, X.M.; Chen, J.Y.; Li, J.J.; Schwegler, B. Characterizing urban fabric properties and their thermal effect using QuickBird image and Landsat 8 thermal infrared (TIR) Data: The case of downtown Shanghai, China. *Remote Sens.* **2016**, *8*, 541. [CrossRef]
78. Li, Y.Y.; Deng, Y.Y.; Chen, Y.S.; Zhang, H. Characterization of Urban Green Space Thermal Environmental Effects Based on Satellite Remote Sensing: A Case Study of Hefei, China. *Ecol. Environ. Sci.* **2018**, *27*, 40–49.